HHS Public Access

Author manuscript

Cancer Discov. Author manuscript; available in PMC 2019 July 31.

Published in final edited form as:

Cancer Discov. 2017 November ; 7(11): 1248–1265. doi:10.1158/2159-8290.CD-17-0401.

Recurrent tumor cell-intrinsic and -extrinsic alterations during MAPKi-induced melanoma regression and early adaptation

Chunying Song[#1,6], **Marco Piva**[#1,6], **Lu Sun**[#1,6], **Aayoung Hong**[1,2,6], **Gatien Moriceau**[1,6], **Xiangju Kong**[1,6], **Hong Zhang**[1,6], **Shirley Lomeli**[1,6], **Jin Qian**[1,6], **Clarissa C. Yu**[1,6], **Robert Damoiseaux**[2,5,6], **Mark C. Kelley**[7], **Kimberley B. Dahlman**[8], **Philip O. Scumpia**[1], **Jeffrey A. Sosman**[9], **Douglas B. Johnson**[9], **Antoni Ribas**[2,3,4,5,6], **Willy Hugo**[1,6], **Roger S. Lo**[1,2,5,6]

[1]Division of Dermatology, Department of Medicine, University of California, Los Angeles, California 90095-1662 USA.

[2]Department of Molecular and Medical Pharmacology, University of California, Los Angeles, California 90095-1662 USA.

[3]Division of Hematology & Oncology, Department of Medicine, University of California, Los Angeles, California 90095-1662 USA.

[4]Division of Surgical Oncology, Department of Surgery, University of California, Los Angeles, California 90095-1662 USA.

[5]Jonsson Comprehensive Cancer Center, University of California, Los Angeles, California 90095-1662 USA.

[6]David Geffen School of Medicine, University of California, Los Angeles, California 90095-1662 USA.

[7]Department of Surgery, Vanderbilt-Ingram Cancer Center, Nashville, TN 37232, USA.

[8]Department of Cancer Biology, Vanderbilt-Ingram Cancer Center, Nashville, TN 37232, USA.

[9]Department of Medicine, Vanderbilt-Ingram Cancer Center, Nashville, TN 37232, USA

[#] These authors contributed equally to this work.

Abstract

Treatment of advanced ^{V600}*BRAF* mutant melanoma using a BRAF inhibitor (BRAFi) or its combination with a MEKi typically elicits partial responses. We compared the transcriptomes of patient-derived tumors regressing on MAPKi therapy against MAPKi-induced temporal transcriptomic states in human melanoma cell lines or murine melanoma in immune-competent mice. Despite heterogeneous dynamics of clinical tumor regression, residual tumors displayed highly recurrent transcriptomic alterations and enriched processes, which were also observed in MAPKi-selected cell lines (implying tumor cell-intrinsic reprogramming) or in bulk mouse tumors (and the CD45-negative or –positive fractions,, implying tumor cell-intrinsic or stromal/immune

Correspondence Author: Roger S. Lo, 52-121 CHS Dept. of Medicine/Dermatology, 10833 Le Conte Ave, Los Angeles, CA 90095-1750; rlo@mednet.ucla.edu.

Authors declare no conflicts of interest.

alterations, respectively). Tumor cell-intrinsic reprogramming attenuated MAPK-dependency, while enhancing mesenchymal, angiogenic and IFN-inflammatory features and growth/survival dependence on multi-RTKs and PD-L2. In the immune compartment, PD-L2 upregulation in CD11c+ immunocytes drove the loss of T-cell inflammation and promoted BRAFi resistance. Thus, residual melanoma early on MAPKi therapy already displays potentially exploitable adaptive transcriptomic, epigenomic, immune-regulomic alterations.

INTRODUCTION

The only clinically validated approach (i.e., BRAFi+MEKi) to suppress acquired BRAFi resistance in melanoma addresses only MAPK-reactivating mechanisms (1–7). Recent appreciation of the pervasiveness of non-genomic and immune evolution in melanoma with acquired or late MAPKi resistance (2) suggests dynamic and continuous alterations early on therapy. This is consistent with the clinical experience that the majority of initial tumor responses to MAPKi are partial, with many acquired resistant tumors later growing *in situ* from these residual tumors. The equilibrium between the tumor cell and stromal/immune compartments is expected to be highly dynamic immediately after initiating therapy. Thus, there is a need to develop models that would recapitulate temporally either tumor cell-intrinsic or -extrinsic adaptations in regressing/persisting melanoma early during MAPKi therapy.

It is known that melanoma tumors responding to MAPKi therapy display robust T-cell infiltration (8). However, the extent and nature of stromal/immune compartment remodeling and potential adaptations, including adaptive immune resistance, has not been systematically characterized in regressing tumors responding to targeted therapy. Compensatory survival signaling, through therapy-induced relief of feedback inhibition on the MAPK pathway (9) and rebound upregulation of the PI3K-AKT pathway (10, 11), has been shown to participate as adaptive mechanisms. However, it is not clear whether early adaptation of melanoma to MAPKi is limited to compensatory signaling or involves transcriptomic or epigenomic reprogramming. Recently, tumor cell mesenchymal transition has been linked to an immune-suppressive microenvironment (12, 13), wound-healing signatures and innate anti-PD-1 resistance (14). Thus, in theory, large-scale phenotypic changes of tumor cells in response to targeted therapy can have profound effects on the tumor microenvironment and anti-tumor immunity. We postulated that macroscopic or clinically evident tumor shrinkage occurs in parallel with the development of therapy tolerance followed by microscopic foci of resistance. In this case, understanding subclinical resistance evolution may offer insights into combinatorial therapeutic targets to suppress such early resistance.

Despite the heterogeneous kinetics of melanoma regression and timing of tumor biopsies on MAPKi therapy, we sought insights into the early adaptive landscape by cataloging recurrent gene and gene set expression alterations across patient-matched tumors on-treatment (On-Tx) vs. pretreatment (Fig. 1A). Across distinct tumors or patients, transcriptome reprogramming, if any, may transit at variable rates along successive stages. Thus, we captured temporally dynamic transcriptomic states by profiling ^{V600}*BRAF* mutant human melanoma cell lines or immune-competent murine melanoma tumors after increasing

durations of continuous MAPKi exposure (Fig. 1B). To nominate tumor cell-intrinsic and -extrinsic (stromal/immune) transcriptomic alterations, we compared regressing clinical tumors against *in vitro*-treated human melanoma cell lines and *in vivo*-treated murine melanoma tumors, respectively. To analyze stromal/immune transcriptomic alterations in murine melanoma, we subtracted transcriptomic alterations in the CD45-negative subpopulation from those in the bulk regressing tumors. We also provided proof-of-concept functional studies to support adaptive, tumor cell-intrinsic and/or -extrinsic roles of RTK or PD-L2 upregulation.

RESULTS

Detection of transcriptomic reprogramming associated with MAPK-redundant resistance in patient-derived melanoma regressing on MAPKi

We obtained patient-matched, melanoma tumors (total n = 46) before MAPKi therapies (BRAFi, MEKi, or BRAFi+MEKi) at baseline (n = 20) and On-Tx (n = 26; 23/26 biopsies on day 22 or earlier) after objective clinical responses (Fig. 1A; Supplementary Table S1A (15)). Residual melanoma cells in "responding" (versus baseline) tumors showed marked decreases in Ki-67 staining or proliferation (Supplementary Fig. S1A). *In vitro,* BRAFi-sensitive ^{V600E}*BRAF* melanoma cell lines on continuous BRAFi treatment reached a population nadir, consisting of slow-cycling, drug-tolerant persisters (DTPs), prior to resuming growth as drug-tolerant proliferating persisters (DTPPs) (Fig. 1B) (11, 16). In most cell lines examined, DTPs acquired a flattened morphology and displayed senescence-associated β-galactosidase (SA-βGal) activity, which was later lost in fibroblastoid DTPP cells (Supplementary Fig. S1B–S1D) (3, 11).

To delineate dynamic transcriptomic states, we profiled parental (P) cell lines treated with DMSO/vehicle, temporal sub-populations (2 d, DTP, DTPP) (days to weeks on BRAFi), and long-term sub-lines (months to years on BRAFi or BRAFi+MEKi, resulting in single-drug resistant or SDR or double-drug resistant or DDR R-lines, respectively) (Fig. 1B; Supplementary Fig. S1E, S1F). We then performed unsupervised clustering based on the top 3,000 most variant genes expressed by 18 isogenic P- versus R-lines (SDR or DDR) (Fig. 1C). Two major clusters emerged: one group of R-lines clustered with all the P-lines; another group of R-lines clustered away from their isogenic P-lines. The group of R-lines clustering with all the P-lines harbored specific drivers of MAPK-reactivation/addiction (i.e., ^{V600E}*BRAF* ultra-amplification, M249 DDR4; ^{V600E}*BRAF* amplification+^{F129L}*MEK1*, M249 DDR5; ^{V600E}*BRAF* splicing, M397 SDR and M395 SDR1; ^{V600E}*BRAF* amplification, M395 SDR2; ^{MUT}*NRAS*, M249 SDR (3, 5, 6, 17)). The second group of R-lines displayed transcriptomic reprogramming, relatively weak ^{V600E}*BRAF* signature enrichment, and attenuated MAPK-dependency (Supplementary Fig. S1G, S1H). Thus, there are two distinct functional and transcriptomic classes of MAPKi resistance: Resistance with MAPK-activation or Ra versus Resistance with MAPK-redundancy or Rr. Accordingly, we observed from Principle Component Analysis (PCA) two temporal transcriptomic trajectories: (1) for Rr, successive transcriptomic reprogramming away from MAPKi-sensitive isogenic P-lines (positioned at the origin) and (2) for Ra, transient transcriptomic

re-programming followed by re-establishment of a transcriptomic state closely matching the isogenic P-lines (Fig. 1D).

We then assessed how transcriptomic changes within On-Tx or disease progressive (DP) tumors (versus patient-matched baseline tumors) would compare relative to the PC trajectory observed for Rr lines (Fig. 1E). Notably, in contrast to the heterogeneous patterns of DP tumors, nearly all On-Tx tumors shifted with the directionality of the DTP->DTPP->Rr trajectory, suggesting converging phenotypes. To understand the biological processes Rr transcriptomic reprogramming, we performed Gene Ontology (GO) enrichment analysis of up- or down-expressed genes unique to each stage, overlapping between two consecutive stages or among all three stages (Fig. 1F, 1G). For example, DTP was characterized by enhanced neural differentiation; DTPP by enhanced interferon signaling; and Rr by reduced melanocyte differentiation. Also, up-expressed genes shared by DTPP and R or all three stages enriched for cytokine signaling/migration or ECM remodeling/angiogenesis. In contrast, Ra cells displayed few unique or overlapping differentially expressed genes (DEGs) (Supplementary Fig. S1I). Thus, BRAFi can induce temporally distinct transcriptomic and phenotypic states leading to MAPK-redundant resistance.

Recurrent tumor cell-intrinsic alterations, including an epigenetically driven mesenchymal-angiogenic switch, in melanoma regressing on MAPKi

Using gene signatures unique to or shared by DTP, DTPP, and Rr states, we detected recurrent and often concurrent positive enrichments in the On-Tx tumors (Fig. 2A). We assessed the significance of transcriptomic similarity between the On-Tx tumors and Rr-lines and found 533 up- and 457 down-expressed genes being shared between On-Tx tumors (≥ 50% of biopsies) and DTP, DTPP, Rr cells (> 50% of cell samples in any of the states) (Fig. 2B; Supplementary Table S2A, S2B). This overlap of DEGs was significant across all pair-wise comparisons (Supplementary Table S2A). The 533 up-expressed genes shared across tumor/cell line samples were enriched for the GO terms “extracellular matrix organization,” “response to IFNA,” “neuron projection,” and “mesenchyme development” (Fig. 2C). Although On-Tx (versus baseline) tumors harbored higher immune/stromal contents (Supplementary Fig. S2A), the significant overlap of their DEGs with those in MAPKi-treated cell lines suggests that the mesenchymal phenotype could arise, in part, tumor cell-autonomously.

We listed the gene set (C2/6, Molecular Signature Database) which were enriched in On-Tx tumors (≥ 50% of biopsies) and any of the *in vitro* temporal stages (Fig. 2D). We observed no gene set recurrently enriched (positive or negative) among the Ra transcriptomes. The top gene sets positively enriched were related to cancer-associated fibroblasts/mesenchymal transition, ECM, IFN/IRF3 and JNK/TNF signaling. Consistently, network analysis of lineage-specific transcription factors (TFs) and target genes (CellNET) (18) showed that Rr lines expressed more fibroblast-specific TFs and target genes (Supplementary Fig. S2B)., For recurrently (> 50%) differentially expressed mesenchymal, neural crest and melanocytic genes found during *in vitro* evolution (Supplementary Table S2C), we observed corresponding DEG patterns in On-Tx tumors (Supplementary Fig. S2C to S2E). The heterogeneity of DEG patterns in neural crest-melanocytic differentiation observed in On-Tx

tumors may be related to heterogeneous intra-tumoral abundance of *MITF*-high versus *MITF*-low, *AXL/NGFR*-high melanoma cells in treatment-naïve tumors (19). We validated BRAFi-induced altered differentiation states based on protein levels of *TFAP2A*, *MITF*, *FOXD3*, *CD271/NGFR*, *ZEB2*, *SNAI2*, and *TAGLN/SM22* (Supplementary Fig. S2F to S2I). Consistent with therapy-induced changes in chromatin regulators of melanoma cell lines (10, 16, 20, 21), we observed highly dynamic temporal expression patterns of chromatin regulator genes, including changing ratios of the atypical histone splice variants *mH2A1.1* and *mH2A1.2,* during BRAFi resistance development (Supplementary Fig. S2J to S2N). Mutually exclusive splicing of *mH2A1.1* versus *mH2A1.2* is known to regulate cancer cell senescence (e.g., heterochromatin, secretory phenotype) and developmental genes (22, 23).

We then sought an epigenomic perspective of the invasive/mesenchymal switch in Rr-lines versus On-Tx tumors. We first analyzed published RNA-seq and H3K27ac-seq data derived from proliferative (n=9) and invasive (n=2) short-term melanoma cultures (Supplementary Fig. S2O) (24). Rr-lines clustered with the invasive group and MAPK-addicted P- and Ra-lines with the proliferative group. Because CpG methylation levels at H3K27ac peaks were generally anti-correlated with H3K27ac levels (24), we determined the differential CpG methylation levels of Rr-lines at the sites of differential H3K27ac specific to invasive versus proliferative cultures. In both On-Tx tumors and Rr-lines, we observed general hyper-methylation at proliferative phenotype-associated H3K27ac peaks and an admixture of hypo- and hyper-methylation at invasive phenotype-associated H3K27ac peaks (Fig. 2E, 2F). Temporally in cell lines (Supplementary Fig. S2P, S2Q), differential CpG methylation at invasive-proliferative switch-associated H3K27ac sites was stage-dependent, being evident starting in DTPPs. Furthermore, we analyzed the correlation between differential CpG methylation and expression of proximal genes in Rr-lines at the proliferative versus invasive H3K27ac peaks (Supplementary Table S2D). At proliferative H3K27ac peaks, most genes (e.g., *MITF, DCT, SOX10*, and *MLANA*) were hyper-methylated and down-expressed (Fig. 2G) and enriched for “pigmentation during development” and “melanocyte differentiation.” At invasive H3K27ac peaks, most genes were up-expressed, enriching for angiogenic and pro-motility processes. Interestingly, the up-expressed invasive genes associated with either hyper- (e.g., *FBN½, EGFR*) or hypo- (e.g., *AXL, EPHA2*) methylation at CpG sites or both hyper- and hypo-methylation at distinct CpG sites within the same genes (e.g., *LOXL2, WNT5A, VEGFC*). Thus, Rr-lines and On-Tx residual melanoma tumors undergo an epigenome-based mesenchymal-invasive-angiogenic switch.

MAPK-redundant resistance displays up-expression of functionally redundant RTKs and PD-L2 in melanoma cells

To identify gene-level consequences of MAPKi-induced tumor cell-intrinsic transcriptomic reprogramming, we rank-ordered the recurrence of mRNA up- and down-expression in On-Tx tumors based on those genes displaying DEG in > 50% of any *in vitro* temporal stage (Fig. 3A; Supplementary Table S2B). DEG was highly concordant among the DTP-DTPP-Rr stages but discordant between Rr and Ra groups. Importantly, recurrence of DEG in On-Tx tumors was highly consistent with those observed during *in vitro* transriptomic evolution of the Rr phenotype. Among the top 50 recurrently up-expressed genes were those involved

in immunity, inflammation, wound healing, cell motility, as well as growth and differentiation. Many up-expressed genes constituted (e.g., *GAS6, LGALS9, IL34, IL32, IL15*) a shared secretome response (Supplementary Fig. S3A and Table S3A). *PDGFRB* up-expression has been shown to be highly recurrent during disease progression (2) and was also highly recurrent early On-Tx, suggesting an adaptive role. Including only RTK genes that met minimal expression cutoff (FPKM ≥ 1) and dynamic range (inter-quartile range (IQR) ≥ 2-fold), we found that Rr-lines formed a distinct cluster from all Ra-lines and P-lines (Supplementary Fig. S3B). Including only RTK genes meeting a cutoff ≥ 2 fold-change (FC) in expression (≥ one pair-wise comparison; IQR ≥ 2), we identified RTKs with DEG in MAPK-redundant growth (Supplementary Fig. S3C). RTKs up-expressed by Rr-lines and On-Tx tumors were supra-physiologic (i.e., above pretreatment levels) in range (Fig. 3B; Supplementary Fig. S3D, S3E). Among RTK genes recurrently up-expressed during DTP-DTPP-Rr evolution, *PDGFRB* (3) and other RTK genes (*AXL*, *c-MET, EGFR*) have been linked to MAPKi-resistance (2, 11, 25, 26). Using validated antibodies (Supplementary Fig. S3F), we detected PDGFRB up-expression as tumor cell-intrinsic and concurrent with EGFR or c-MET up-expression (Fig. 3C).

As in On-Tx tumors, PDGFRB, EGFR, c-MET and AXL in cell lines displayed supra-physiologic and concurrent up-expression in Rr- (but not Ra-) lines, along with higher p-AKT but lower p-ERK levels (Supplementary Fig. S4A). We then tested whether concurrent PDGFRB and EGFR supra-physiologic up-expression could result in PDGFBB-dependent EGFR-transactivation. After serum starvation, PDGF-BB treatment induced strongly p-PDGFRB, p-EGFR, p-AKT, and p-ERK levels in M229 and M238 SDR-lines (versus P-lines) (Supplementary Fig. S4B). This PDGF-BB->PDGFRB->EGFR signaling did not depend on the kinase activity of PDGFRB, as sunitinib (PDGFRBi) treatment inhibited PDGF-BB-induced p-PDGFRB levels but not p-EGFR accumulation. Interestingly, downstream p-AKT and p-ERK induction was attenuated but not abolished (Supplementary Fig. S4C). However, co-treatment of the Rr-lines with gefitinib (EGFRi) on top of PDGF-BB and sunitinib strongly reduced PDGF-BB-induced p-AKT and p-ERK levels and their clonogenic growth (Supplementary Fig. S4D, S4E).

Among immune-regulomic genes (Supplementary Table S3A) with DEG coherent between On-Tx tumors and DTP-DTPP-Rr temporal evolution were immune checkpoint genes such as *PDCD1LG2/PD-L2, CD274/PD-L1 and LAG3*. IFN signatures were enriched positively starting at DTPP *in vitro*, but, unlike in On-Tx tumors, there was no up-expression of IFNA/B/G (Supplementary Fig. S5A). This finding suggested that tumor cell-intrinsic IFN pathway activation in response to MAPKi could remodel the tumor immune microenvironment independently of an adaptive response to anti-tumor T-cells. In On-Tx tumors, T-cell infiltration occurred along with a wholesale immune compartment expansion (Supplementary Fig. S5B and Table S3B), consistent with a tissue injury or wound-healing response, and with a lower ratio *CD8A* to CD8 T-cell exhaustion or checkpoint inhibitory genes (Supplementary Fig. S5C). Since eventual disease progression is commonly associated with loss of CD8 T-cell inflammation (2), the MAPKi-“responsive” phase may be a window of opportunity to augment anti-tumor immunity and suppress resistance development.

Among the top recurrently up-expressed immune genes, *PD-L2* was expressed at a supra-physiologic range (Fig. 3E, 3F). Methylation levels (FC or absolute levels) at a specific CpG site in *PD-L2* were significantly anti-correlated with mRNA levels in this melanoma tissue and cell line cohort and TCGA melanoma (Fig. 3G). The identified *PD-L2* CpG site lost methylation with increasing duration of BRAFi selection and *PD-L2* mRNA expression (Fig. 3H and Supplementary Fig. S5D, S5E) and located within H3K27ac peaks of short-term invasive melanoma cultures (Fig. 3I). Moreover, PD-L2 (versus PD-L1) protein up-expression in Rr-lines (versus P-lines) was more robust; neither PD-L1 or -L2 was up-expressed in Ra-lines (Fig. 3J; Supplementary Fig. S5F to S5H). In paired frozen tumors, we observed strong PD-L2 protein up-expression in residual tumor cells on-MAPKi (Fig. 3K). Thus, PD-L2, which has not been shown as a preclinical or clinical target in cancer, may in fact be relevant therapeutically in the context of MAPKi-induced immune phenotypic switch.

Tumor cell-intrinsic PD-L2 up-expression promotes survival of *in vitro* models of MAPK-redundant resistance

Given a reported tumor cell-intrinsic, anti-apoptotic role of PD-L1 (27), we first assessed a potential tumor cell-intrinsic, adaptive function of PD-L2's supra-physiological expression by testing whether *PD-L2* knockdown by shRNAs in Rr-lines would suppress clonogenic growth and induce apoptosis (Fig. 4A, 4B; Supplementary Fig. S6A to S6C). Indeed, partial knockdown of PD-L2 levels in Rr-lines by five independent shRNAs consistently and strongly reduced clonogenic growth and induced apoptosis. Interestingly, co-culture with HEK293T cells expressing PD-1 attenuated or rescued basal or PD-L2 knockdown-induced apoptosis in Rr-lines (Supplementary Fig. S6D; Fig. 4C, 4D), which was reversed by co-expression of soluble PD-L2 in HEK293T cells (Supplementary Fig. S6E, S6F). Additionally, we induced apoptosis in Rr-lines with staurosporine (STP) prior to co-cultures (with STP washed away before co-culture) and observed that PD-1 expression by neighboring cells protected Rr-lines from basal and STP-induced apoptosis (Fig. 4E). This PD-1-mediated protection of apoptosis was not observed in the P-lines or Ra-lines, which did not up-express PD-L2 (Supplementary Fig. S6G and S6H). Thus, PD-L2 up-expression promotes survival of MAPK-redundant resistance tumor cell-intrinsically and in a manner augmented by interaction with PD-1.

To gain insights into tumor cell-intrinsic anti-apoptotic processes mediated by PD-L2-PD-1 interaction, we sorted two Rr-lines (based on negative GFP expression) in the baseline growth condition or after brief STP treatments from co-cultures with HEK293T cells with or without PD-1 over-expression. PCA of RNA-seq data generated from non-apoptotic, GFP-negative Rr cells showed that STP treatment was associated with a negative shift along the PC2 axis (Fig. 4F), where PC2 positive-driving genes were enriched for cell cycle progression and PC2 negative-driving genes were enriched for cell death genes (Supplementary Fig. S6I). While this reflected the effects of STP-pretreatment on gene expression, we also observed that, regardless of STP-pretreatment, co-culture with PD-1-expressing cells invariably resulted in a positive shift along PC3 (Fig. 4F), where PC3 positive-driving genes were enriched for angiogenic processes and PC3 negative-driving genes were enriched for inflammation (Fig. 4G). Thus, binding of PD-1 with PD-L2

expressed by Rr-lines may reduce the apoptotic propensity of melanoma cells under chronic MAPKi treatment stress by suppressing tumor cell-intrinsic inflammation, a potential mechanism corroborated by gene set enrichment analysis (Supplementary Fig. S6J) and further by *in vivo* experiments (see below).

MAPKi remodels the stromal/immune compartment with PD-L2 up-expression in CD11c-positive immunocytes

We also assessed gene- and gene signature-level consequences of MAPKi-induced tumor stromal/immune compartment remodeling by comparing clinical On-Tx tumors to immune-competent murine melanoma temporally transcriptome-profiled after BRAFi treatment. A syngeneic, transplantable murine melanoma model (YUMM1.7 *Braf/Pten/Cdkn2a* mutant cells subcutaneously transplanted into C57BL/6 mice) was used for this comparative transcriptomic analysis, but the clinical relevance of this murine melanoma model was first assessed. YUMM1.7 tumors regressed soon after daily gavage with BRAFi (vemurafenib), and residual tumors persisted before resuming growth (Fig. 5A). Transcriptomes derived from vehicle-treated tumors (day 3 or d3) and BRAFi-treated tumors at d6 (regressing), d15 (residual) and d30 (re-growing) were analyzed for expression levels of *CD8A/B* and CD8 T-cell activation/cytolytic genes (Fig. 5B). This analysis showed heterogeneous but progressive induction of CD8 T-cell activation/cytolytic genes early on-treatment, which peaked in the residual, maximally regressed tumors. Tumor re-growth, however, was associated with loss of CD8 T-cell inflammation. We also observed progressive enrichment of a set of signatures related to Innate anti-PD-1 Resistance (IPRES) (14), reflecting hypoxia, TGFβ1 signaling and mesenchymal transition. Enrichment of inflammatory and IFN-induced signatures corresponded to up-expression of *CD8A/B*, peaked in maximally regressed YUMM1.7 tumors on BRAFi but ceased when the tumors re-grew. Thus, YUMM1.7 tumors in response to BRAFi therapy recapitulated the transcriptomic evolution of clinical melanoma.

We first determined in patient-derived On-Tx tumors the differential expression patterns of immune genes recurrently and coherently up- or down-expressed in any stage (regressing, residual or progressing) of YUMM1.7 tumors on BRAFi (Fig. 5C; Supplementary Table S2B). By rank-ordering up-expressed immune genes in clinical On-Tx tumors based on the frequency of recurrence (Fig. 5C), we could appreciate the immune-regulomic similarity between On-Tx tumors and regressing/residual (but not progressing) YUMM1.7 tumors. To define tumor cell-intrinsic versus -extrinsic immune-regulomic alterations, we annotated the recurrence profile (Fig. 5C) with DEG patterns in the CD45-negative fraction of residual YUMM1.7 tumors and in human melanoma cell samples (i.e., DTP, DTPP, Rr or Ra). We first determined that DEG (in particular gene up-expression) overlapped significantly between MAPKi-selected human cell lines *in vitro* and the CD45-negative fraction of mouse tumors *in vivo* (Supplementary Fig. S7A). These overlapping up-expressed genes enriched for GO terms such as ECM organization and cell migration. Additionally, a gene set enrichment analysis that incorporated recurrent alterations in the CD45-negative fraction of residual YUMM1.7 tumors (Supplementary Fig. S7B) revealed concordant and recurrent enrichment of cancer-associated fibroblast (CAF), mesenchymal transition and ECM-remodeling signatures in On-Tx tumors, DTP-DTPP-Rr temporal populations, and CD45-negative residual YUMM1.7 tumors. By excluding the characteristic MAPKi-induced

(tumor cell-intrinsic) transcriptomic alterations observed in human melanoma cell lines *in vitro* and in the CD45-negative fraction of residual YUMM1.7 tumors, we nominated the majority of recurrent gene up-expression in On-Tx tumors (Fig. 5C) as tumor cell-extrinsic alterations. Consistently, at the gene signature enrichment level (Fig. 5D), the top recurrently enriched gene signatures in the On-Tx tumors, with support in any of the temporally sampled YUMM1.7 tumors, were all related to immune cell function, indicating wholesale immune cell infiltration (including CD8 T-cells) as during wound-healing. Interestingly, loss of CD8 T-cell noted earlier (Fig. 5B) in progressing YUMM1.7 tumors was accompanied by loss of pan-immune subsets (Fig. 5D). While the top recurrently up-expressed immune genes in On-Tx tumors were not commonly attributable to the tumor cell compartment, the top recurrently up-expressed genes in general (including the secretome, Supplementary Fig. S3A) were frequently attributable to the CD45-negative residual YUMM1.7 tumor cells or DTP-DTPP-R subpopulations *in vitro* (Supplementary Fig. S7C).

By comparing results in Figures 3D versus 5C, we noted a few exceptions where recurrent immune gene (e.g., *CD36*, *CXCL12*, and *CD274/PD-L1*) up-expression in On-Tx tumors may be attributable, at least partially, to tumor cell-driven up-expression. We also noticed that, while *PDCD1LG2/PD-L2* was up-expressed robustly during the DTP-DTPP-Rr evolution in human melanoma cell lines (Fig. 3), it was not in the CD45-negative fraction of residual YUMM1.7 tumors (Fig. 5C). In fact, the full-length *PD-L2* transcript was detected by RNA-seq only with sufficient intra-tumoral inflammation (e.g., when YUMM1.7 tumors were treated with BRAFi) (Supplementary Fig. S7D). As a cell line in response to BRAFi treatment, YUMM1.7 expressed only the 3’ short transcript, which is missing the 5’ exons required to translate the extra-cellular domain (Supplementary Fig. S7E, S7F). Thus, this model presented an opportunity to assess the impact of PD-L2 induction specifically in the immune compartment. Furthermore, in YUMM1.7 tumors, we confirmed by Ki-67 and CD8 quantitative immunofluorescence highly dynamic alterations in proliferative status and intra-tumoral CD8 T-cells abundance (Fig. 5E, 5F). We also confirmed Pd-l2 accumulation and observed its frequent co-localization with CD11c (a myeloid dendritic marker) in the immune compartment of regressing/residual YUMM1.7 tumors (Fig. 5G).

Pd-l2 blockade in the immune compartment prolongs BRAFi response and CD8 T-cell accumulation

Importantly, co-treatment of BRAFi with a Pd-l2-blocking antibody (aPD-L2) consistently delayed growth of resistant tumors, while aPD-L2 monotherapy did not lead to tumor growth inhibition or shrinkage (Fig. 6A, 6B; Supplementary Fig. S7G to S7I). We hypothesized that aPD-L2 acts by delaying the loss of CD8 T-cell inflammation that occurs during the evolution of BRAFi resistance. Consistently, at d33, BRAFi+aPD-L2-responsive tumors, compared to tumors that have escaped either BRAFi alone or BRAFi+aPD-L2, displayed the highest number of CD8 T-cells (Fig. 6C). We also profiled via RNA-seq YUMM1.7 tumors that have escaped BRAFi (n=3), BRAFi+aPD-L2 (n=2) or remained responsive to BRAFi+aPD-L2 (n=2) at d33 (Fig. 6D) and compared their PC positions relative to those from the BRAFi-treatment time course (Fig. 5A). From this transcriptomic perspective, we found that d33 YUMM1.7 tumors that remained responsive to BRAFi+aPD-L2 segregated with d15 residual tumors on BRAFi alone, while d33 tumors that escaped

BRAFi or BRAFi+aPD-L2 shifted positively along the PC1 axis toward d30 BRAFi-treated tumors (Fig. 6D). To understand this pattern further, we analyzed the GO term enrichments of PC1- and PC1+ driving genes and found that the former genes enriched for T-cell immunity while the latter for proliferation (Fig. 6E). Moreover, we harvested YUMM1.7 tumors before the tumors sizes differed significantly between the treatment groups (Supplementary Fig. S7J) and quantified the intra-tumoral CD8 T-cell numbers. Consistent with the hypothesis that aPD-L2 acts by delaying the loss of CD8 T-cell inflammation, we found that, in the residual tumors, aPD-L2 co-treatment already led to a significantly higher number of CD8 T-cells (Fig. 6F). Also, as MAPKi induced infiltration by Pd-l2-positive immunocytes early during tumor regression, we expected and observed that delayed aPD-L2 (versus BRAFi) treatments reduced its efficacy (Supplementary Fig. S7K). Moreover, aCD8 neutralization (Supplementary Fig. S7L) reduced the tumor-control efficacy of BRAFi+aPD-L2 but not of BRAFi alone (Supplementary Fig. S7M, S7N), suggesting that in this model CD8 T-cells contribute effective anti-tumor immunity only with Pd-l2 blockade in the immune compartment.

Pd-l2 over-expression tumor cell-intrinsically promotes BRAFi resistance in an immunodeficient microenvironment

Since BRAFi-induced Pd-l2 expression in the immune compartment promoted melanoma adaptation in a T-cell-dependent fashion, we next examined whether tumor cell-intrinsic Pd-l2 expression could promote BRAFi resistance in an *in vivo* but immune deficient microenvironment (i.e., NOD scid gamma or NSG mice). Since YUMM1.7 melanoma cells lack full-length *Pd-l2* expression, we engineered Pd-l2 over-expression and, after subcutaneous transplantation, assessed tumor growth in NSG mice (n=8 tumors per group). Pd-l2 over-expression in YUMM1.7 melanoma cells did not significantly alter tumor growth in mice treated with the vehicle, but, with BRAFi treatment, accelerated resistance development (Fig. 7A). Histologically, BRAFi-treated YUMM1.7 tumors (at d19; three tumors nearest the median weight were selected) with Pd-l2 over-expression (versus no over-expression) displayed more densely packed sheets of spindled malignant appearing cells (Fig. 7B). Blinded quantification of mitotic figures along with histiocytes and granulocytes revealed significantly higher levels of mitosis but lower levels of infiltration by histiocytes and granulocytes with Pd-l2 over-expression (Fig. 7C), consistent with distinct tumor sizes and suggestive of tumor cell cross-talk with innate immune cells. Analysis of the RNA-seq profiles of tumors from all four groups (n=3 per group) showed highest *Pd-l2* levels in the two groups with exogenous over-expression. We also observed BRAFi-inducible *Pd-l2* up-expression in the control vector group, likely from the limited immune microenvironment. Regardless of BRAFi treatment, we also observed enhanced levels of the immune-suppressive factor *VEGFA* with *Pd-l2* over-expression (Fig. 7D), the latter of which was confirmed at the protein level on the cell surface (Fig. 7E). PCA of the RNA-seq data suggested that PC2 positive- and negative-driving genes and their functional pathways as critical to the tumor cell-intrinsic effects of Pd-l2 in an immunodeficient *in vivo* environment (Fig. 7F). In this model, BRAFi negatively shifted the tumor transcriptomes along the PC2 axis, regardless of *Pd-l2* expression status, while *Pd-l2* over-expression positively shifted the tumor transcriptomes along PC2, “reversing” the effect of BRAFi. PC2 positive-driving genes were enriched for hypoxia and other processes, whereas PC2 negative-driving genes

were enriched for inflammatory processes (Fig. 7G). Consistent with these results, gene set enrichment analysis showed that *Pd-l2* over-expression (regardless of BRAFi treatment) led to positive enrichment of hypoxia gene signatures and negative enrichment of multiple IRF-dependent and immunocyte signatures (including those of histiocytes and granulocytes) (Fig. 7H). Thus, melanoma tumor cell-intrinsic over-expression of Pd-l2 accelerates BRAFi resistance even in an immunodeficient *in vivo* microenvironment, potentially through upregulating hypoxia-driven oncogenic processes and downregulating inflammatory signaling. The growth/survival benefits of these modulations may be unmasked by BRAFi treatment.

DISCUSSION

The scale and nature of tumor cell-intrinsic and -extrinsic alterations, during the early course of MAPKi therapy for advanced melanoma, have not been defined systematically. This view is essential to start to address the potential adaptive nature of these changes and define therapeutic opportunities. We integrated transcriptomic analysis of patient-matched pretreatment and regressing/residual melanoma with analysis of MAPKi-induced temporal transcriptomic alterations in human melanoma cell lines *in vitro* and murine melanoma tumors in an immune-competent context. By focusing on recurrent transcriptomic alterations during each stage of response/adaptation in the experimental models, we uncovered similar highly recurrent gene and gene program expression alterations in patient-derived On-Tx tumors. These recurrent transcriptomic alterations originated in the tumor cell and/or immune compartment, as inferred by concordant changes in 1) On-Tx clinical tumors versus human cell lines (i.e., putative tumor cell-intrinsic alterations) or 2) On-Tx versus mouse tumors (but absent in the CD45-negative fraction of mouse tumors, i.e., putative tumor cell-extrinsic alterations). This approach incorporating temporal dynamics in experimental systems enhanced our view of heterogeneous On-Tx clinical tumors, which were biopsied at varied times and responded to therapy with distinct kinetics. Importantly, this integrative analysis of patient-derived tumors and experimental systems enabled functional interrogation of clinically relevant and highly ranked alterations in patient tumors as potentially adaptive and targetable responses.

This study identified regressing/residual melanoma “responsive” to MAPKi therapy as a nidus of dynamic transcriptomic-CpG methylomic reprogramming and of tumor cell persistence and resistance through attenuated MAPK-dependency. MAPK-redundant tumor growth control by multi-RTK up-regulation associated with a mesenchymal/invasive/angiogenic switch, highlighting therapeutic challenges. Recent pan-cancer studies (12–14) have linked mesenchymal, angiogenic, and immune-suppressive transcriptomic features, which together are associated with clinical innate (14) and adaptive (28) anti-PD-1 resistance in melanoma. Thus, MAPKi induction of such microenvironmental alterations, including CD8 T-cell infiltration, reflect an immune phenotypic switch that presages loss of T-cell inflammation and likely loss of anti-PD-1 responsiveness. In the immune-competent context, MAPKi should induce release by tumor cells of danger-associated molecular patterns (DAMPs), which would promote non-infectious inflammation. Surviving malignant cells appear to undergo mesenchymal/angiogenic/fibroblastic transition and, through an expanded secretome and cell-surface expression of immune-modulatory molecules, actively

participate in chronic wound-healing or inflammation, which is immune-suppressive. Hence, it may be critical to disrupt this immune-phenotypic transition early during “successful” MAPK-targeted therapy in order to prevent the eventual loss of T-cell inflammation.

As a proof-of-concept, we showed that, by inducing infiltration of PD-L2-expressing immunocytes and tumor cell-intrinsic PD-L2 up-expression, BRAFi unmasks PD-L2’s pro-tumorigenic and -resistance function. This function of PD-L2 expressed by non-tumor cells in the immune microenvironment is at least partially dependent on its ability to down-regulate intra-tumoral CD8 T-cell function and/or number. Tumor cell-intrinsic PD-L2 up-expression and its interaction with PD-1 increased fitness of melanoma cells epigenomically adapting to MAPKi. Recent work showed that PD-L2 expression, independently of PD-L1 expression, predicted clinical response to pembrolizumab in head and neck squamous cell carcinoma, suggesting that clinical responses to PD-1 blockade may be related partly to blockade of PD-1/PD-L2 interactions (29). It also remains to be determined how much of PD-L2’s tumor cell-intrinsic function is relevant clinically in the context of MAPKi resistance. Further mechanistic understanding and biomarker discovery of PD-L2’s tumor cell-intrinsic function would facilitate this evaluation.

The recognition of tumor cell-intrinsic transcriptomic re-programming and its potential immune-suppressive, immune-editing or pro-metastatic impacts early during therapy calls for pre-emptive, up-front combinatorial therapies. Although the intrinsic requirement of tumor cell mesenchymal transition for metastatic capability has been called into question (30–32), its importance in early adaptive resistance to targeted therapy is strongly suggested by our study. We also observed, in On-Tx clinical tumors, MAPKi inducing tumor cell-intrinsic (in human melanoma cell lines and the CD45-negative fraction of YUMM1.7 tumors) up-expression of multiple factors that could promote metastasis. One example is the fatty acid receptor CD36, which has been nominated recently (33) as a critical driver of metastasis-initiating cells. Tumor neoantigens can result from somatic mutations or re-expression of cancer testis antigens. MAPKi-induced epigenomic reprogramming raises the possibility of cancer testis antigens as endogenous immune or exogenous immunotherapeutic targets. Furthermore, immune-suppressive candidates include tumor cell-intrinsic elaboration of TGFβ2, VEGFA/C, and IFN up-regulation. Interestingly, chronic IFN stimulation of tumor cells has been shown to induce T-cell inhibitory receptors and reduce sensitivity to aPD-1 blockade (34). Also, EGFR, VEGF and other triggers of STAT3 signaling could promote immunosuppression (35). Loss of PTEN or induction of AKT has been associated with decreased T-cell infiltration into tumors and T-cell mediated tumor killing through expression of immunosuppressive cytokines (36). Importantly, MAPK-redundant resistance that results from transcriptomic re-programming invariably up-regulates AKT signaling. Thus, further analysis of this data set and exploitation of these experimental models should generate additional combinatorial targets with the potential to tighten the bottleneck of melanoma evolution in response to MAPKi therapy.

METHODS

Analysis of Tumor Specimens

All melanoma tumors (pretreatment, on-treatment) were obtained with the approval of institutional review boards (IRBs) and patients' consents. mRNAs from 24 snap-frozen specimens were extracted by the mirVana RNA Isolation Kit (Life Technologies) and pair-end sequenced with read length of 2×100 bps (Illumina HiSeq2000, unstranded TruSeq RNA Sample Preparation Kit v2), except for patient #9 (2×150 bps, Illumina HiSeq3000, Kapa Stranded mRNA-seq kit) and patient #5 (for which microarray was used). Also, RNASeq data of 22 independent specimens (15) were analyzed in parallel. Selected tumor samples were also subjected to whole-exome sequencing (n=8 pairs) to verify tumor content and to methylome profiling (n=4 pairs) to corroborate methylomic studies of cell lines.

Cell Culture, Sub-line Derivation, Infection, and Treatments

All cell lines were routinely tested for *Mycoplasma*, and cell line and sub-line identities have been ensured by RNA-seq and the GenePrint 10 system (Promega) at routine intervals during the course of this study for banking and experimental studies. All M series cell lines were established from patient-derived tumors at UCLA. SKMEL28 was obtained from Dr. Alan Houghton (between 2008 and 2010). YUMM1.7 was obtained from Dr. Marcus Bosenberg (between 2014 and 2016). All cell lines were maintained in DMEM high glucose with 10% heat-inactivated FBS (Omega Scientific) and 2mM glutamine in humidified, 5% CO_2 incubator. To derive DTPP clones, parental melanoma cells seeded at low density were treated with drugs as indicated every 2–3 days for 3–6 weeks, and highly proliferative colonies were ring-isolated and expanded. SDR and DDR sub-lines were derived previously as stated in Supplementary Methods. ShPD-L2 and vector control (Thermo Fisher) were packaged into lentiviral particles for infection. PD-1-GFP and its empty lentiviral vector were purchased from Origene. See Supplementary Methods for details on all antibody, small molecule inhibitor and growth factor treatments.

Protein Detection

Cells were lysed in RIPA buffer (Sigma) with protease inhibitor cocktail (Roche and phosphatase inhibitor cocktails (Santa Cruz Biotechnology) for Western blotting. Paraffin-embedded formalin-fixed sections were subjected to heat-induced antigen retrieval. The biotin-streptavidin system (Vector Laboratories) and DAB were used to visualize human Ki-67, while Alexa Fluor conjugates (Life Technologies) and TSA plus fluorescein system (Perkin Elmer) were used to detect human PDGFRβ, EGFR, c-MET and mouse ki-67, PD-L2, CD8 and CD11c. For immuno-cytochemistry, cells were fixed with 4% PFA and stained with Alexa Fluor 555 (for Ki-67) and Alexa Fluor 488 (for CD271) conjugates (Life Technologies). Nuclei were counterstained by hematoxylin or DAPI. Fluorescent images were digitized using the Applied Imaging Ariol SL-50scanner at 20x magnification. Quantification of CD8 and Ki-67 signals was performed using the Definiens Tissue Studio 4.3 (Definiens, Inc.) according to the manufacturer's instruction. Please refer to Supplementary Methods for primary antibody information. Cell surface PD-L1 and PD-L2 were detected by flow cytometry using APC-conjugated anti-PD-L1 and PE-conjugated anti-PD-L2 antibodies (BioLegend).

Cell Line-based Assays

Senescence was assessed by senescence-β-galactosidase staining kit (Cell Signaling Technologies). CSFE (Molecular Probes) dilution was monitored by flow cytometry to follow cell division. Clonogenic and cell cycle assays are described in Supplementary Methods. For vital imaging, cells were plated onto gridded-dishes (Sigma) and imaged every two days at five pre-designated areas.

Treatment and Analysis of YUMM1.7 Tumors

YUMM1.7 cells (1 million per flank, two flanks per mouse) were subcutaneously implanted into C57BL/6 mice. Tumors were treated with BRAFi when the volumes reached to 150–200mm^3. αPD-L2 antibodies and isotype control were administrated intraperitoneally. Tumors were dissociated into single cells and stained with a αCD45 antibody. The CD45-negative population was sorted for RNA extraction. See Supplementary Methods for additional details.

RNA-seq Analysis of Melanoma Cell Lines and Tumors

FASTQ reads were mapped to the UCSC hg19 or mm9 (for the YUMM1.7 mouse melanoma study) reference genome using Tophat2. Normalized expression levels of genes (and transcripts in the case of *mH2A1.1* and *mH2A1.2*) were expressed in FPKM values as generated by cuffquant and cuffnorm. Since we observed over-expressions of the last two exons in the *Pdcd1lg2* gene without the accompanying expression of the other exons in the YUMM1.7 tumors treated with BRAFi for 30 d, we excluded the reads mapping to the last two exons when we quantified the *Pdcd1lg2* mRNA expression in the YUMM1.7 RNA-seq dataset. A gene was defined as differentially expressed when its expression increased or decreased by at least two-fold for cell lines or 1.5-fold ($|\log_2 FC| \geq 0.585$) for tumors (including YUMM1.7 tumors). To overcome noise in differential expression values caused by extremely low FPKM levels, we added a pseudo-FPKM value of 0.1 to all expression values. Recurrence analysis of up- or down-expressions of genes was performed for cell lines/YUMM1.7 tumors/patient tumors with respect to their parental/vehicle-treated/pretreatment lines or tumors, respectively. We used the ESTIMATE algorithm (37) to calculate the extent of immune infiltration of the baseline and On-Tx tumors based on gene expression data. Tumor purities were called using WES analysis by Sequenza (38). The purities of samples without WES data were estimated by the fraction of Sanger-derived $^{MUT}BRAF$ peaks compared to the WT peaks, assuming heterozygous *BRAF* mutation. Paired gene set enrichment was performed as described (2); single-sample gene set enrichment was quantified using GSVA (39). GO term enrichment was computed based on online functional annotation tool ENRICHR (40). RNA-seq data have been made available through Gene Expression Omnibus (GEO) at the accession number GSE75313.

Analysis of Methylome and H3K27 ChIP-Seq

Differentially methylated CpG sites in tumor/cell line samples (profiled by Illumina 450K Methylation arrays) were computed as described (2). We intersected the proliferative and invasive H3K27ac peak regions (24) with the Illumina 450K Methylation probes. For each peak region with more than one CpG probes, we calculated the median of the methylation

changes across the CpG probes. Using the independently derived H3K27ac signals and methylation changes from our studies, we computed the Pearson correlation between the fold differences of H3K27ac signals (invasive versus proliferative cultures) and % methylation changes (in Rr-lines or On-Tx tumors versus their respective P-lines or pretreatment tumors) of the CpG sites within the H3K27ac peaks. To analyze differential mRNA expression (between Rr- and P-lines) within regions of differential H3K27ac and methylation, we selected those H3K27ac peaks overlapping with one or more differentially methylated CpG sites (q-value ≤ 0.05, $|\Delta\beta| \geq 10\%$) and whose nearest genes were differentially expressed (≥1.5-fold up- or down-expression) in more than half of the Rr-lines. These genes were grouped into four different categories (hypo- or hyper-methylation with mRNA up- or down-expression).

Supplementary Material

Refer to Web version on PubMed Central for supplementary material.

Acknowledgments

We thank G. Bollag (Plexxikon Inc.) for providing PLX4032/4720, M.W. Bosenberg for YUMM1.7, H. Shi for technical assistance, and P. Scumpa for histopathology expertise. We thank all patients who donated tissues for this research. Patient-informed consent was obtained for the research performed in this study.

Grant Support

This work has been funded by Burroughs Wellcome Fund (to R.S. Lo), the National Institutes of Health (1R01CA176111 to R.S. Lo; P01CA168585 to A. Ribas and R.S Lo.; K12CA0906525 to D.B. Johnson), the Ressler Family Foundation (to R.S. Lo and A. Ribas), the Melanoma Research Alliance (to R.S. Lo, D.B. Johnson and W. Hugo), the Ian Copeland Melanoma Fund (to R.S. Lo), the SWOG/Hope Foundation (to R.S. Lo and A. Ribas), Steven C. Gordon Family Foundation (to R.S. Lo), American Skin Association (W. Hugo), American Association for Cancer Research-Amgen, Inc. Fellowship in Clinical/Translational Cancer Research (16-40-11-HUGO to W. Hugo), Department of Defense Horizon Award (to A. Hong), Dermatology Foundation (to G. Moriceau), National Cancer Center Aggressive Cancer Research (to J. Qian), the ASCO Conquer Cancer Career Development Award (to D.B. Johnson), and American Cancer Society Research Professorship (to J.A. Sosman).

REFERENCES

1. Emery CM, Vijayendran KG, Zipser MC, et al. MEK1 mutations confer resistance to MEK and B-RAF inhibition. Proc Natl Acad Sci U S A 2009;106:20411–6. [PubMed: 19915144]
2. Hugo W, Shi H, Sun L, et al. Non-genomic and Immune Evolution of Melanoma Acquiring MAPKi Resistance. Cell 2015;162:1271–85. [PubMed: 26359985]
3. Nazarian R, Shi H, Wang Q, et al. Melanomas acquire resistance to B-RAF(V600E) inhibition by RTK or N-RAS upregulation. Nature 2010;468:973–7. [PubMed: 21107323]
4. Shi H, Hugo W, Kong X, et al. Acquired Resistance and Clonal Evolution in Melanoma during BRAF Inhibitor Therapy. Cancer Discov 2014;4:80–93. [PubMed: 24265155]
5. Shi H, Moriceau G, Kong X, et al. Preexisting MEK1 exon 3 mutations in V600E/KBRAF melanomas do not confer resistance to BRAF inhibitors. Cancer Discov 2012;2:414–24. [PubMed: 22588879]
6. Shi H, Moriceau G, Kong X, et al. Melanoma whole-exome sequencing identifies (V600E)B-RAF amplification-mediated acquired B-RAF inhibitor resistance. Nat Commun 2012;3:724. [PubMed: 22395615]
7. Van Allen EM, Wagle N, Sucker A, et al. The genetic landscape of clinical resistance to RAF inhibition in metastatic melanoma. Cancer Discov 2014;4:94–109. [PubMed: 24265153]

8. Frederick DT, Piris A, Cogdill AP, et al. BRAF inhibition is associated with enhanced melanoma antigen expression and a more favorable tumor microenvironment in patients with metastatic melanoma. Clin Cancer Res 2013;19:1225–31. [PubMed: 23307859]
9. Lito P, Pratilas CA, Joseph EW, et al. Relief of profound feedback inhibition of mitogenic signaling by RAF inhibitors attenuates their activity in BRAFV600E melanomas. Cancer Cell 2012;22:668–82. [PubMed: 23153539]
10. Obenauf AC, Zou Y, Ji AL, et al. Therapy-induced tumour secretomes promote resistance and tumour progression. Nature 2015;520:368–72. [PubMed: 25807485]
11. Shi H, Hong A, Kong X, et al. A Novel AKT1 Mutant Amplifies an Adaptive Melanoma Response to BRAF Inhibition. Cancer Discov 2014;4:69–79. [PubMed: 24265152]
12. Chen L, Heymach JV, Qin FX, Gibbons DL. The mutually regulatory loop of epithelial-mesenchymal transition and immunosuppression in cancer progression. Oncoimmunology 2015;4:e1002731. [PubMed: 26155392]
13. Mak MP, Tong P, Diao L, et al. A Patient-Derived, Pan-Cancer EMT Signature Identifies Global Molecular Alterations and Immune Target Enrichment Following Epithelial-to-Mesenchymal Transition. Clin Cancer Res 2015;9 29:Epub ahead of print.
14. Hugo W, Zaretsky JM, Sun L, et al. Genomic and Transcriptomic Features of Resistance and Sensitivity to Anti-PD-1 Therapy in Metastatic Melanoma. Cell 2016;165:35–44. [PubMed: 26997480]
15. Kwong LN, Boland GM, Frederick DT, et al. Co-clinical assessment identifies patterns of BRAF inhibitor resistance in melanoma. J Clin Invest 2015;125:1459–70. [PubMed: 25705882]
16. Sharma SV, Lee DY, Li B, et al. A chromatin-mediated reversible drug-tolerant state in cancer cell subpopulations. Cell 2010;141:69–80. [PubMed: 20371346]
17. Moriceau G, Hugo W, Hong A, et al. Tunable-Combinatorial Mechanisms of Acquired Resistance Limit the Efficacy of BRAF/MEK Cotargeting but Result in Melanoma Drug Addiction. Cancer Cell 2015;27:240–56. [PubMed: 25600339]
18. Cahan P, Li H, Morris SA, Lummertz da Rocha E, Daley GQ, Collins JJ. CellNet: Network Biology Applied to Stem Cell Engineering. Cell 2014;158:903–15. [PubMed: 25126793]
19. Tirosh I, Izar B, Prakadan SM, et al. Dissecting the multicellular ecosystem of metastatic melanoma by single-cell RNA-seq. Science 2016;352:189–96. [PubMed: 27124452]
20. Kemper K, de Goeje PL, Peeper DS, van Amerongen R. Phenotype Switching: Tumor Cell Plasticity as a Resistance Mechanism and Target for Therapy. Cancer Res 2014;74:5937–41. [PubMed: 25320006]
21. Menon DR, Das S, Krepler C, et al. A stress-induced early innate response causes multidrug tolerance in melanoma. Oncogene 2015;34:4448–59. [PubMed: 25417704]
22. Buschbeck M, Uribesalgo I, Wibowo I, et al. The histone variant macroH2A is an epigenetic regulator of key developmental genes. Nat Struct Mol Biol 2009;16:1074–9. [PubMed: 19734898]
23. Chen H, Ruiz PD, McKimpson WM, Novikov L, Kitsis RN, Gamble MJ. MacroH2A1 and ATM Play Opposing Roles in Paracrine Senescence and the Senescence-Associated Secretory Phenotype. Mol Cell 2015;59:719–31. [PubMed: 26300260]
24. Verfaillie A, Imrichova H, Atak ZK, et al. Decoding the regulatory landscape of melanoma reveals TEADS as regulators of the invasive cell state. Nat Commun 2015;6:6683. [PubMed: 25865119]
25. Girotti MR, Pedersen M, Sanchez-Laorden B, et al. Inhibiting EGF receptor or SRC family kinase signaling overcomes BRAF inhibitor resistance in melanoma. Cancer Discov 2013;3:158–67. [PubMed: 23242808]
26. Muller J, Krijgsman O, Tsoi J, et al. Low MITF/AXL ratio predicts early resistance to multiple targeted drugs in melanoma. Nat Commun 2014;5:5712. [PubMed: 25502142]
27. Azuma T, Yao S, Zhu G, Flies AS, Flies SJ, Chen L. B7-H1 is a ubiquitous antiapoptotic receptor on cancer cells. Blood 2008;111:3635–43. [PubMed: 18223165]
28. Chen PL, Roh W, Reuben A, et al. Analysis of Immune Signatures in Longitudinal Tumor Samples Yields Insight into Biomarkers of Response and Mechanisms of Resistance to Immune Checkpoint Blockade. Cancer Discov 2016;6:827–37. [PubMed: 27301722]
29. Yearley JH, Gibson C, Yu N, et al. PD-L2 Expression in Human Tumors: Relevance to Anti-PD-1 Therapy in Cancer. Clin Cancer Res 2017;23:3158–67. [PubMed: 28619999]

30. Fischer KR, Durrans A, Lee S, et al. Epithelial-to-mesenchymal transition is not required for lung metastasis but contributes to chemoresistance. Nature 2015;527:472–6. [PubMed: 26560033]
31. Harper KL, Sosa MS, Entenberg D, et al. Mechanism of early dissemination and metastasis in Her2+ mammary cancer. Nature 2016.
32. Zheng X, Carstens JL, Kim J, et al. Epithelial-to-mesenchymal transition is dispensable for metastasis but induces chemoresistance in pancreatic cancer. Nature 2015;527:525–30. [PubMed: 26560028]
33. Pascual G, Avgustinova A, Mejetta S, et al. Targeting metastasis-initiating cells through the fatty acid receptor CD36. Nature 2017;541:41–5. [PubMed: 27974793]
34. Benci JL, Xu B, Qiu Y, et al. Tumor Interferon Signaling Regulates a Multigenic Resistance Program to Immune Checkpoint Blockade. Cell 2016;167:1540–54 e12. [PubMed: 27912061]
35. Yu H, Kortylewski M, Pardoll D. Crosstalk between cancer and immune cells: role of STAT3 in the tumour microenvironment. Nat Rev Immunol 2007;7:41–51. [PubMed: 17186030]
36. Peng W, Chen JQ, Liu C, et al. Loss of PTEN promotes resistance to T cell-mediated immunotherapy. Cancer Discov 2015;12 8:Epub ahead of print.
37. Yoshihara K, Shahmoradgoli M, Martinez E, et al. Inferring tumour purity and stromal and immune cell admixture from expression data. Nat Commun 2013;4:2612. [PubMed: 24113773]
38. Favero F, Joshi T, Marquard AM, et al. Sequenza: allele-specific copy number and mutation profiles from tumor sequencing data. Ann Oncol 2015;26:64–70. [PubMed: 25319062]
39. Hanzelmann S, Castelo R, Guinney J. GSVA: gene set variation analysis for microarray and RNA-seq data. BMC Bioinformatics 2013;14:7. [PubMed: 23323831]
40. Chen EY, Tan CM, Kou Y, et al. Enrichr: interactive and collaborative HTML5 gene list enrichment analysis tool. BMC Bioinformatics 2013;14:128. [PubMed: 23586463]

SIGNIFICANCE

Incomplete MAPKi-induced melanoma regression results in transcriptome/methylome-wide reprogramming and MAPK-redundant escape. Although regressing/residual melanoma is highly T-cell-inflamed, stromal adaptations, many of which tumor cell-driven, could suppress/eliminate intra-tumoral T-cells, reversing tumor regression. This catalog of recurrent alterations helps identify adaptations like PD-L2 operative tumor cell-intrinsically and/or extrinsically early on-therapy.

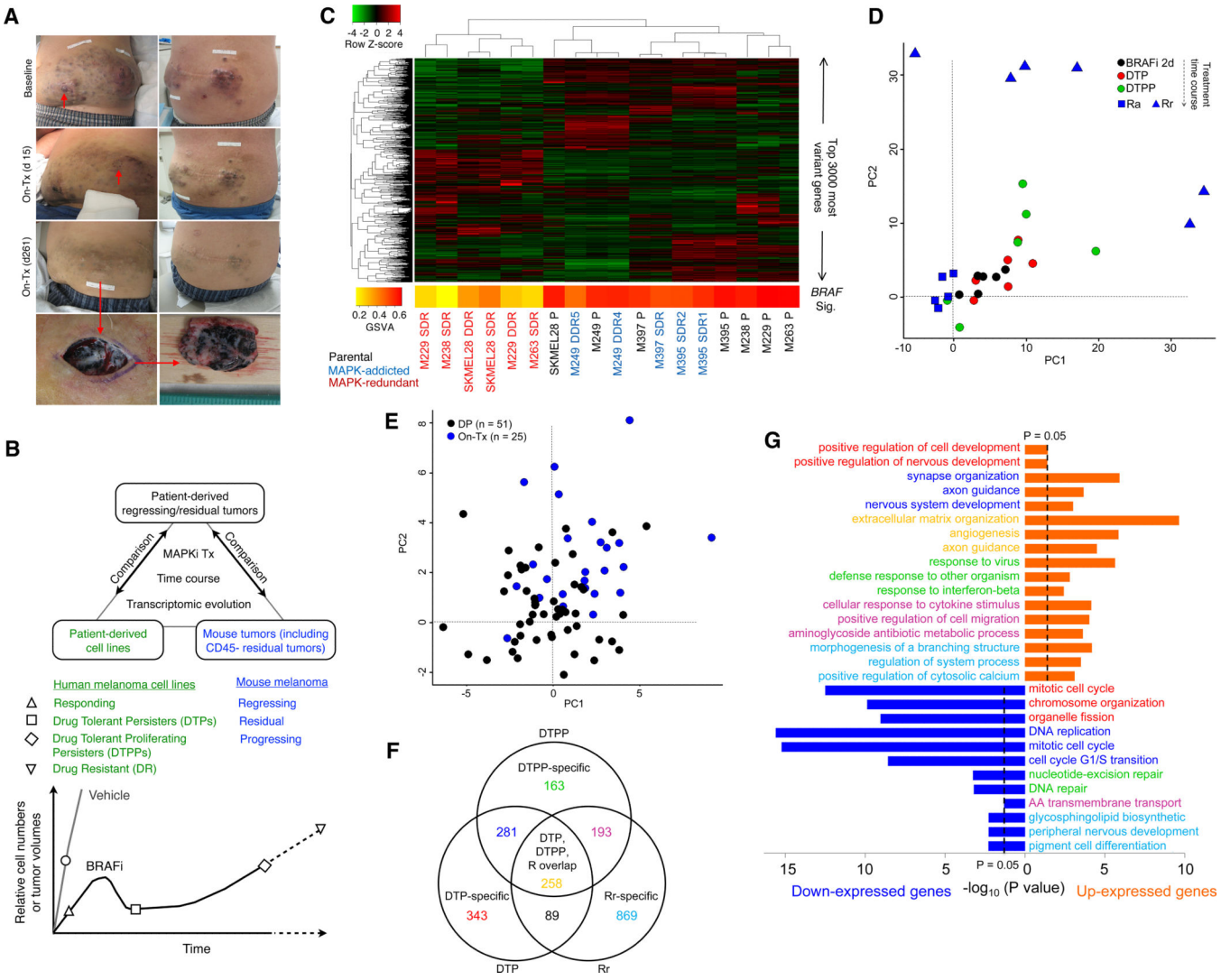

Figure 1.

Nongenomic evolution within regressing/residual clinical tumors on MAPKi therapy. **A,** Clinical photos of MAPKi therapy (patient #4) showing a partial response and serial tumor biopsies. **B,** Overall study design of comparative transcriptomic analysis of gene expression alterations in On-Tx tumors (relative to patient-matched baseline tumors) versus gene expression alterations at multiple time points (after initiating MAPKi treatment) in human melanoma cell lines or murine melanoma tumors. **C,** Heat map showing unsupervised hierarchical clustering based on top variant gene expression levels of parental lines (P-line) and isogenic single drug–resistant (SDR) or double drug–resistant (DDR) lines. Bottom, GSVA enrichments of a *BRAF*MUT signature. **D,** PCA of BRAFi-induced temporal transcriptomic states in *BRAF*MUT melanoma cell lines (P-lines at origin; Ra, resistance with MAPK addiction; Rr, resistance with MAPK-redundancy; Ra or Rr lines include SDR and DDR lines). **E,** Projection of transcriptomes from pretreatment tumors (origin) versus patient-matched On-Tx or disease progression (DP) tumors onto the PC½ space in **D**. **F,** Numbers of up-expressed genes (fold change ≥ 2) in >50% of drug-tolerant persister (DTP),

drug-tolerant proliferating persister (DTPP), or Rr lines and their pattern of overlap. **G,** GO (biological processes) enrichments of temporal stage-specific or overlapping up-expressed and down-expressed (FC ≥ 2) genes in DTP, DTPP, and Rr lines.

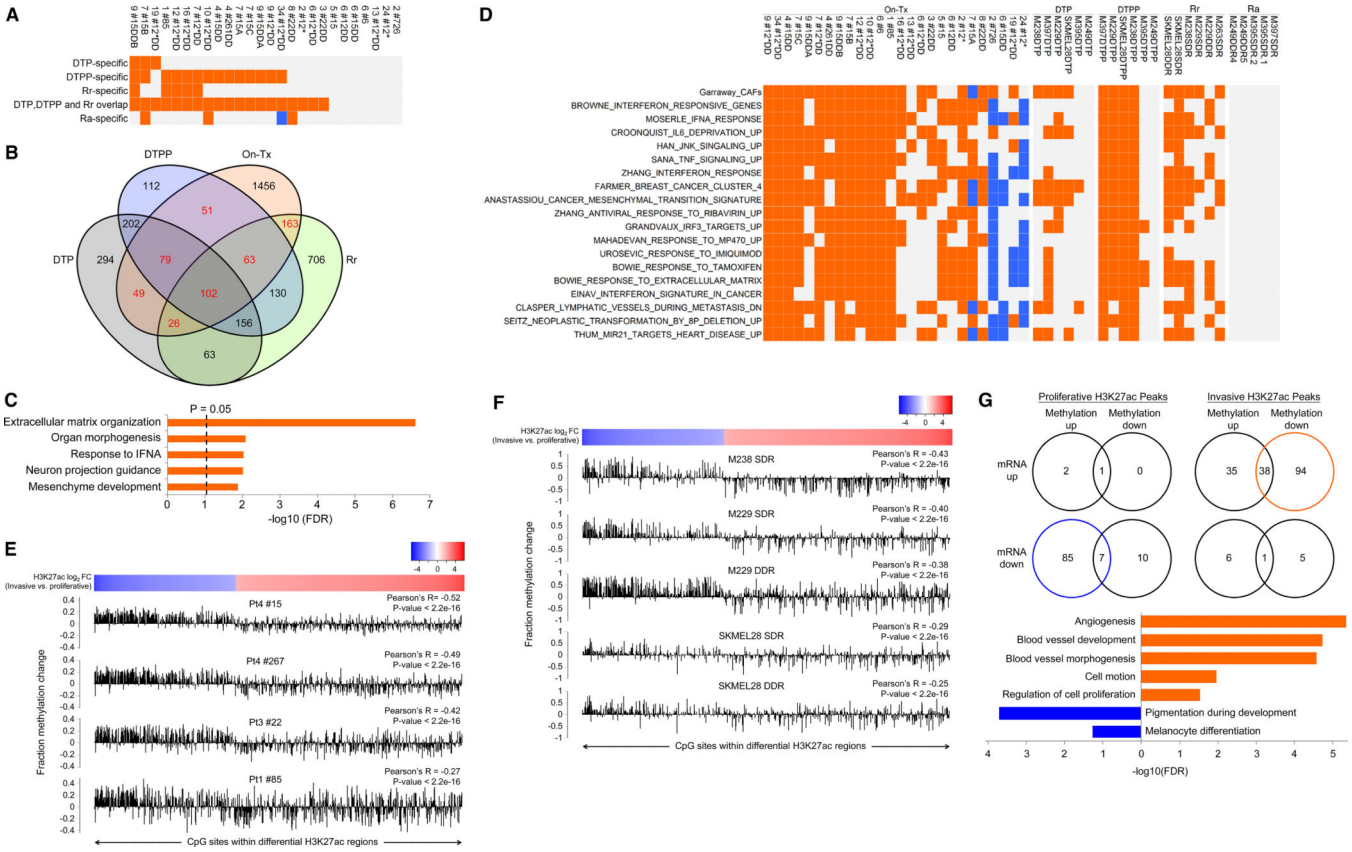

Figure 2.

MAPKi-induced transcriptomic and methylomic alterations shared by patient-derived regressing tumors and cell lines with temporal transcriptomic reprogramming. **A,** Recurrent enrichment of cell line–derived, stage-specific, and stage-overlapping signatures (see Fig. 1F) across On-Tx tumors from patients. Orange, positive enrichment; blue, negative enrichment. **B,** Numbers of genes recurrently up-expressed (>50% of cell line samples; 2-fold) in DTP, DTPP, or Rr lines versus On-Tx tumors (≥50% of tissue samples; 1.5-fold) and their overlaps. **C,** GO enrichments of overlapping up-expressed genes in **B** (red numbers). **D,** Enrichment pattern across On-Tx tumors of gene sets recurrently (>50%) enriched within any of the DTP, DTPP, Rr, or Ra set of samples. **E** and **F,** Changes in CpG methylation levels in On-Tx versus baseline tumors in **E** or SDR or DDR Rr lines versus isogenic P-lines in **F** at chromosome locations of differential H3K27ac peaks between invasive and proliferative melanoma cultures. R, Pearson correlation between differential CpG methylation and log2 fold change (FC) of H3K27ac levels. *P, t* test. **G,** Number of genes proximal to H3K27ac peaks with indicated differential mRNA (FC ≥ 1.5) and CpG methylation ($|\Delta\beta| \geq 10\%$, FDR adjusted $P \leq 0.05$) patterns in Rr lines in **F**. Bottom, GO enrichments of genes within blue and orange circles.

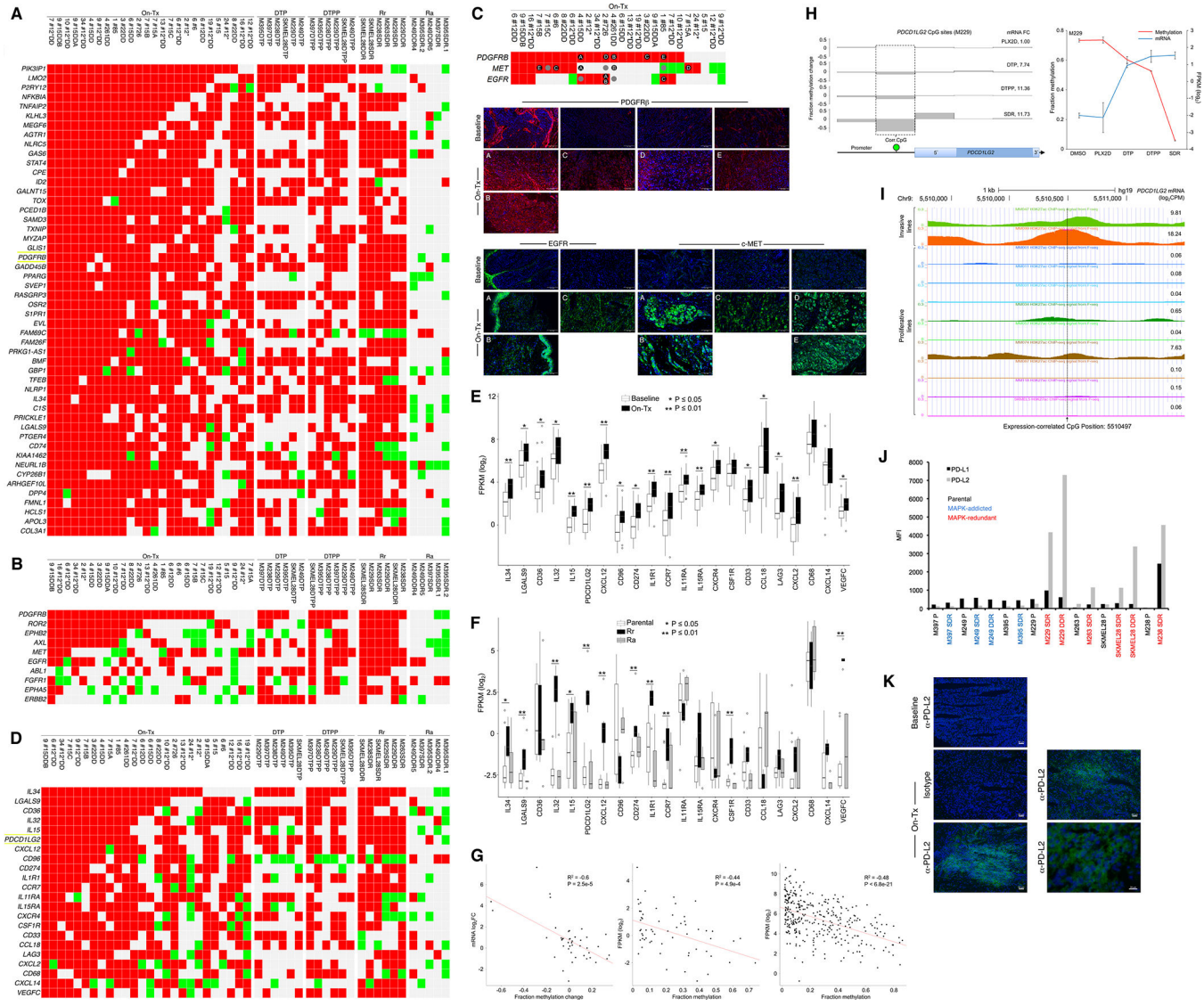

Figure 3.

Recurrent tumor cell–intrinsic transcriptomic, RTKinomic, and immune regulomic alterations in regressing melanoma on MAPKi therapy. **A, B,** Pattern of differential expression of genes in the On-Tx tumor samples with recurrent (>50%) up-expression in any of the DTP, DTPP, Rr, or Ra set of samples (**A**, top 50 genes; **B,** RTK genes only; red and green, up-expression and down-expression). **C,** Immunofluorescence of PDGFRβ, EGFR, and c-MET using formalin-fixed, paraffin-embedded (FFPE) tumor tissues designated by letters (ruler, 100 μm); negative staining by gray circles. **D,** As in **A** and **B** except showing only top recurrently up-expressed immune regulomic genes. **E** and **F,** Expression ranges of immune genes in **D** among baseline versus On-Tx tumors (**E**) or P versus Rr or Ra lines (**F**). **G** (left), Correlation between FCs in *PD-L2* mRNA expression and % methylation changes at the expression anticorrelated CpG site of *PD-L2* across comparisons of DP versus baseline tumors and Rr versus P lines. Middle, correlation across all samples (from the left panel) and (right) all TCGA melanoma samples. R, Pearson correlation coefficient; *P*,

Student *t* test. **H,** Methylation changes at all profiled CpG sites (green bubble, expression-correlated site; left) or absolute methylation levels at the expression-correlated CpG site (right) versus *PD-L2* mRNA expression FC (left) or absolute levels (right). All changes relative to vehicle-treated M229. **I,** H3K27ac chromatin immunoprecipitation sequencing (ChIP-seq) peaks covering the *PD-L2* expression–correlated CpG site in invasive versus proliferative melanoma cultures. *PD-L2* mRNA levels also shown. **J,** Median fluorescence intensities (MFI) of PD-L1 and PD-L2 staining in P versus Rr or Ra lines. **K,** PD-L2 immunofluorescence using frozen tissues from patient #3 (100× scale bar, 50 μm; 400× scale bar, 20 μm). Several views shown for On-Tx tumor.

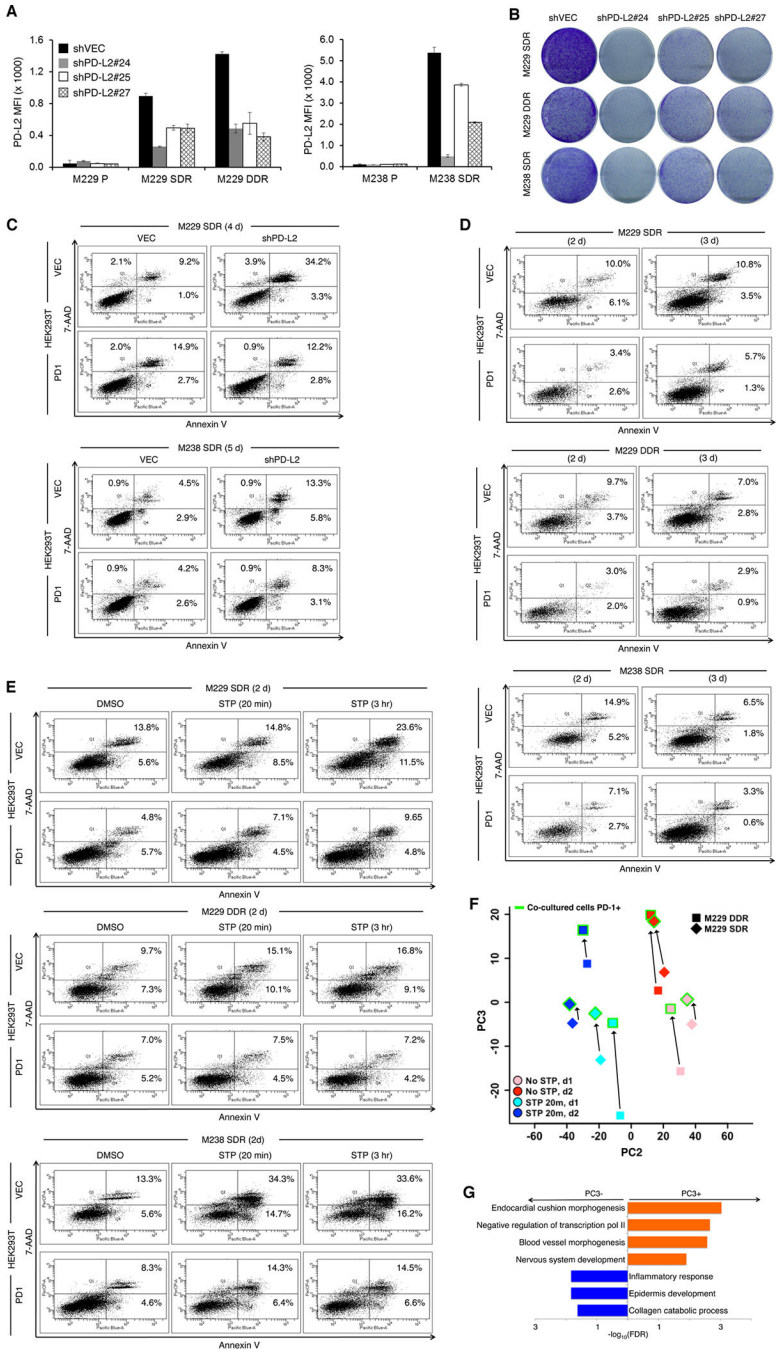

Figure 4.

PD-L2 upregulation promotes tumor cell–intrinsic MAPKi resistance. **A,** PD-L2 surface detection in P and Rr lines with stable expression of empty vector (shVec) or sh*PD-L2*. Error bars, SEM. **B,** Clonogenic growth of indicated Rr lines, with shVec or indicated sh*PD-L2*, for 9 days. Quantifications relative to each cell line culture with shVec. **C,** Apoptosis (%) in Rr lines stably expressing shVec or sh*PD-L2* #9 + #24 on indicated days after lentiviral infection. GFP- (VEC) or PD-1–GFP-expressing HEK293T cells were added to melanoma cell cultures on day 2 of infection at a ratio of 1 to 2. **D,** Apoptosis on indicated days in Rr

lines cocultured from the outset with GFP- (VEC) or PD-1–GFP-expressing HEK293T cells at a ratio of 2 to 1. **E,** Apoptosis on day 2 in Rr lines pretreated with DMSO or staurosporine (STP; 0.5 μmol/L) for 20 minutes or 3 hours, washed free of STP, and then cocultured with GFP- (VEC) or PD-1–GFP-expressing HEK293T cells at a ratio of 2 to 1. **F,** PCA of RNA-seq profiles of indicated Rr lines pretreated with DMSO or STP (0.5 μmol/L) for 20 minutes, washed free of DMSO/STP, and cocultured with GFP- (VEC) or PD-1–GFP-expressing HEK293T cells for 1 or 2 days. Live Rr cells were sorted as GFP-negative cells and then RNA-seq profiled. **G,** GO enrichment analysis of the PC3− and PC3+ driving genes from **F**.

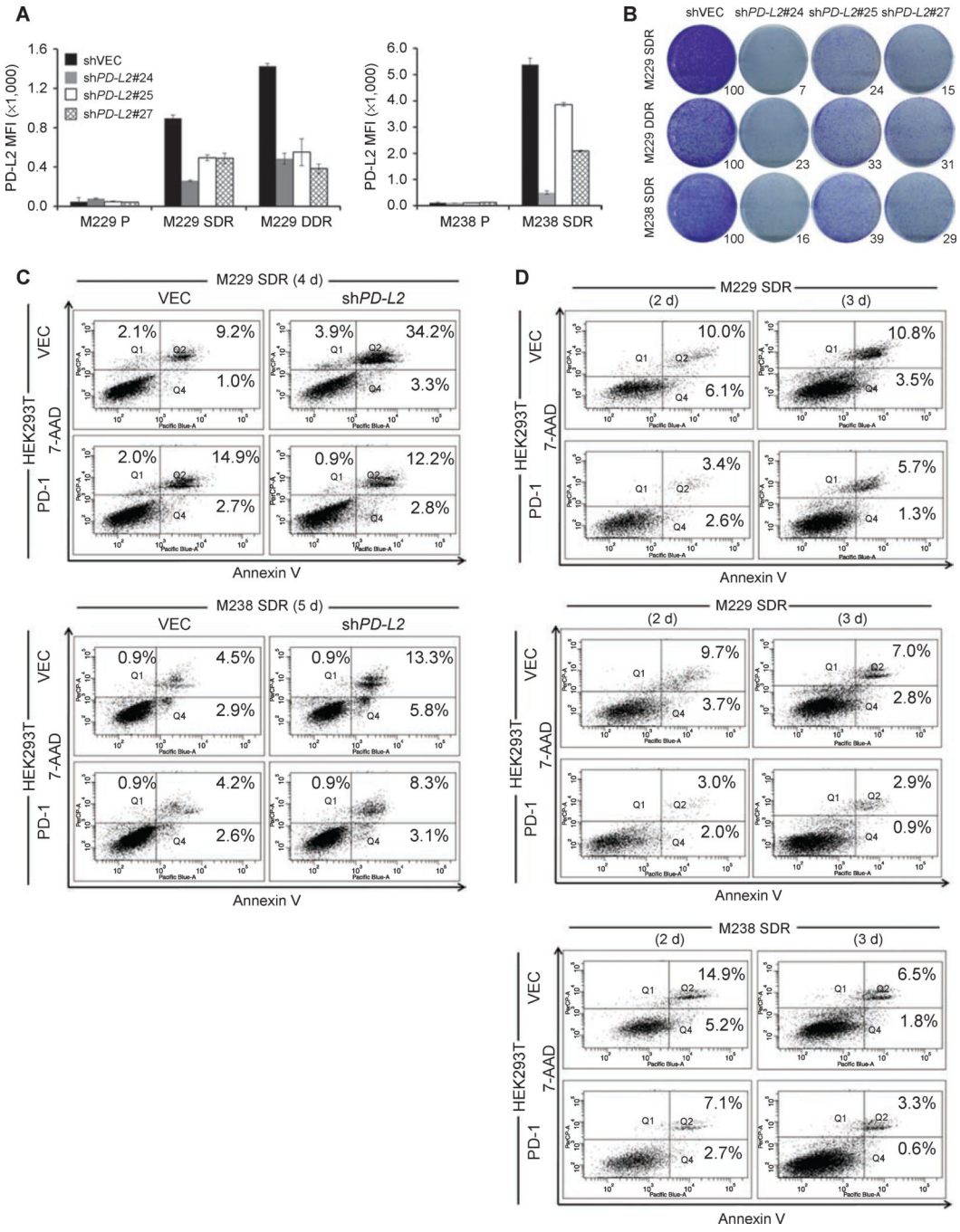

Figure 5.

Recurrent transcriptomic alterations in the tumor immune microenvironment of regressing melanoma on MAPKi therapy. **A,** YUMM1.7 tumor volumes with vehicle (100% DMSO) versus BRAFi (vemurafenib, 100 mg/kg/d gavage) treatment ($n = 8$ per group; mean and error bars, SEM). **B,** Gene set variance analysis and differential gene expression in vehicle versus BRAFi-treated YUMM1.7 tumors from **A**. **C,** On-Tx tumor profile of un-expressed immune-regulomic genes with support of recurrent un-expression (>50%) in any of the regressing, residual, or progressing set of YUMM1.7 tumors. Also shown is the pattern of

differential expression in the CD45-negative fraction of residual YUMM 1.7 tumors and in any of the cell line samples (DTP, DTPP, or Rr) from Fig. 3A. **D,** Pattern of enrichment in On-Tx tumors (rank ordered by recurrence frequency of positive enrichment) of gene sets with support from YUMM1.7 tumors as in **C**. **E,** Representative scanned and quantified images of Ki-67/CD8 immunofluorescence of tumor sections from **A** (DAPI, nuclear counterstain). **F,** Ki-67 or CD8 quantifications from **E** (n = 5 tumors per time point; 2–3 regions per tumor; error bars, SEM; Student t test, P values: *, ≤0.05; **, ≤0.01; n.s., not significant; reference, DMSO 3 d). **G,** Immunofluorescent costaining of CD11c and PD-L2 of tumor sections from **A** (scale bar, 20 μm). Representative low and high magnification images shown.

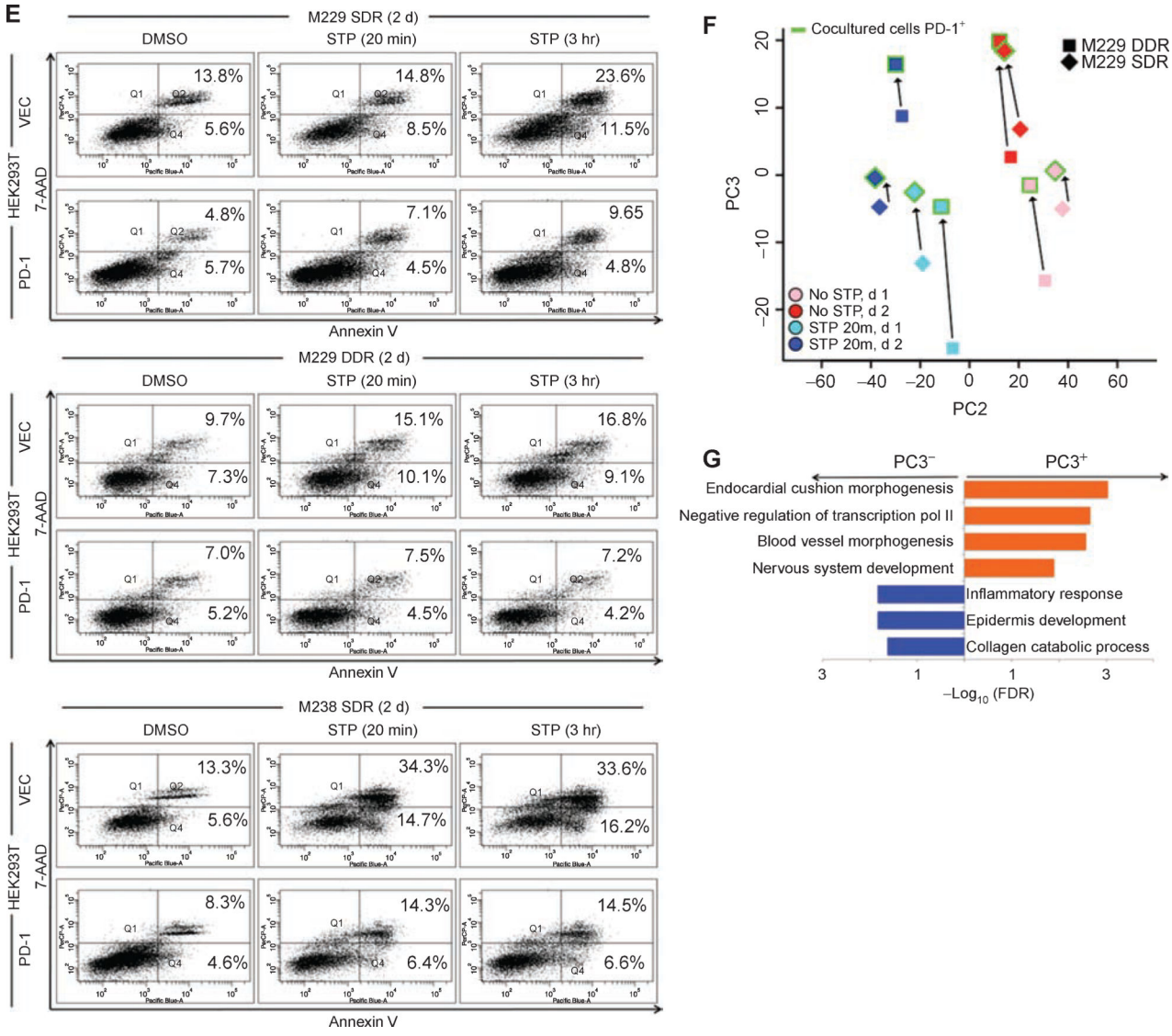

Figure 6.

PD-L2 blockade delays BRAFi resistance in murine melanoma by enforcing a CD8+ T cell–inflamed residual tumor state. **A,** YUMM1.7 tumor volumes with indicated treatments (vehicle, 0.1% methylcellulose and 10% DMSO; BRAFi, vemurafenib 100 mg/kg/d gavage; isotype (iso) or aPD-L2 antibody at 300 μg/mouse twice per week i.p.; $n = 8$ per group; error bars, SEM). Data representative of three independent experiments. **B,** Progression-free survival (cutoff tumor size at ≥150% of size at treatment initiation) of mice in **A**. *P* values, log-rank test. **C,** Tumors from experiment in **A** harvested on day 33 available as FFPE tissue for CD8 and Ki-67 quantifications ($n = 6$, 2, and 4 tumors, BRAFi + isotype, BRAFi + aPD-L2 responsive, BRAFi + aPD-L2, unresponsive, respectively; 3 regions per tumor; error bars, SEM; Student *t* test, *P* values: **, ≤0.01; n.s., not significant; reference, BRAFi + isotype). **D,** Tumors from experiment in **A** with available RNA-seq profiles analyzed by PCA along with RNA-seq profiles derived from tumors in Fig. 5A. **E,** GO enrichment analysis of PC1− and PC1+ driving genes from **D**. **F,** YUMM1.7 tumors treated with BRAFi

+ isotype ($n = 6$) or BRAFi + aPD-L2 ($n = 8$), harvested on day 8, and analyzed by CD8 and Ki-67 immunofluorescence. Quantification, 3 regions per tumor; error bars, SEM; Student t test, P values: *, ≤0.05; reference, BRAFi + isotype.

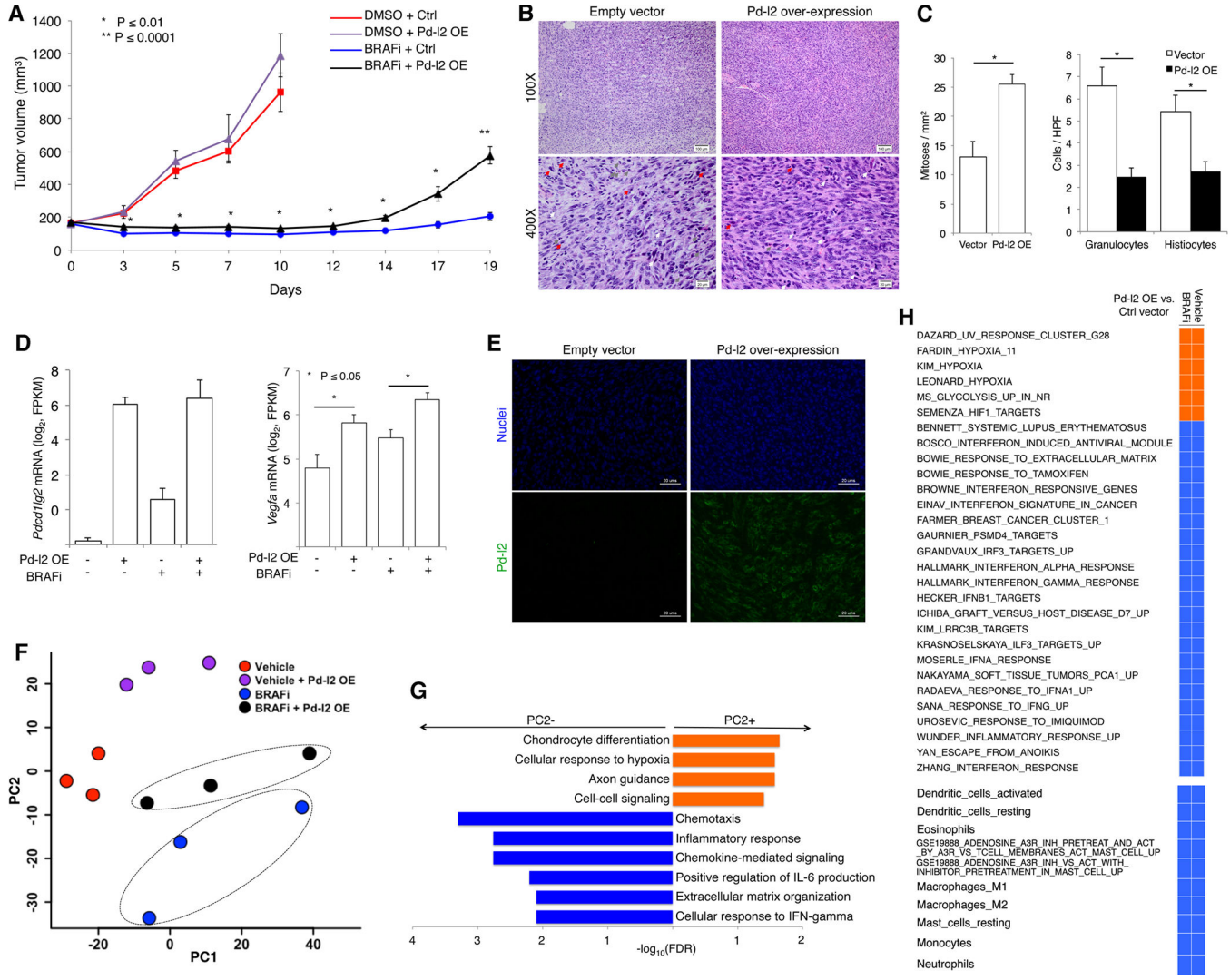

Figure 7.

Tumor cell–intrinsic PD-L2 overexpression promotes BRAFi resistance independently of CD8+ T cells. **A,** Tumor volumes of YUMM1.7 [engineered *in vitro* with control (Ctrl) vector or PD-L2 overexpression (OE)] following treatment with vehicle (0.1% methylcellulose, 10% DMSO) or BRAFi (chow containing PLX4720 at 417 ppm). Vehicle, $n = 8$; BRAFi, $n = 10$; error bars, SEM; *P* values, Student *t* test. Data are representative of two independent experiments. **B,** Representative hematoxylin and eosin images of BRAFi-treated tumors from **A** at d19 (white arrows, mitotic figures; red, histiocytes; grey, granulocytes; 100× scale bar, 100 μm; 400× scale bar, 20 μm. **C,** Blinded quantifications of (left) mitosis and (right) histiocytes and granulocytes [average from 10 high power fields (HPF) $n = 3$ tumors per BRAFi-treated group; error bars, SEM; *P* values, Student *t* test]. **D,** *Pd-l2* and *Vegfa* mRNA levels of indicated YUMM1.7 tumor groups. Error bars, SEM; *P* values, Student *t* test. **E,** Representative immunofluorescent staining of VEGFA in BRAFitreated tumors (scale bar, 20 μm). **F,** PCA of RNA-seq profiles from indicated tumor groups ($n = 3$ tumors nearest the median tumor weights per group). **G,** GO enrichment

analysis of the PC2− and PC2+ driving genes from **F**. **H,** Gene set enrichment analysis of YUMM1.7 tumors with or without PD-L2 OE (in both vehicle- and BRAFi-treated conditions; top, Molecular Signature Data Base signatures; bottom, immune cell marker signatures.